PRESSURE DROP MEASUREMENT OF LAMINAR AIR FLOW IN PROTOTYPIC BWR AND PWR FUEL ASSEMBLIES

E. Lindgren and S. Durbin

Sandia National Laboratories
Albuquerque, New Mexico

Abstract

For this study, dry air at ambient conditions was metered into the bottom of two unheated prototypic fuel assembly mock-ups. One assembly was a 17×17 PWR and the other was a 9×9 BWR fuel assembly. Pressure drop measurements were made in the laminar regime with Reynolds numbers ranging from 10 to 1000. High sensitivity quartz crystal differential pressure gauges capable of detecting slight changes in differential pressure with a resolution of ~0.02 Pa provided meaningful pressure drop measurements across individual grid spacers and bundle segments.

With fewer grid spacers and expanded flow area in the upper bundle, the BWR assembly exhibited less flow resistance at a given Reynolds number compared to the PWR assembly when located in a tight storage cell sized to be analogous to the BWR canister. The tight PWR storage cell was smaller than any used commercially in spent fuel pools or dry storage casks. When the PWR assembly was tested inside of storage cell sizes that spanned pool and cask cells available in industry, the flow resistance at a given Reynolds number was equivalent to or less than that exhibited by the BWR assembly.

1 INTRODUCTION

To the knowledge of the authors, these studies are the first hydraulic characterizations of a full length, highly prototypic fuel assemblies in low Reynolds number flows (DeStordeur, 1961; Rehme, 1973; Cheng and Todreas, 1986; Todreas and Kazimi, 1990). The advantages of full scale testing of prototypic components are twofold. First, the use of actual hardware and dimensionally accurate geometries eliminates any issues arising from scaling arguments. Second, many of the prototypic components contain intricacies by design that would not be reproduced by using simplified flow elements. While this approach yields results that are inherently specific to the fuel assembly under testing, the differences in commercial designs are considered minor, particularly when considering the hydraulics of the entire assembly.

In a previous study the hydraulic characterization of a full scale, highly prototypic boiling water reactor (BWR) assembly mockup was conducted using state-of-the-art quartz crystal differential pressure gauges (Lindgren and Durbin, 2007). These pressure gauges have an unprecedented resolution of ±0.02 N/m^2 (±0.000003 psi) that allows accurate measurement of the pressure drops across assembly segments at very low Reynolds numbers (Re = 60 to 900 for the BWR study).

These studies found the resistance to flow in the BWR assembly was significantly greater than predicted by generally assumed and accepted best estimate "textbook" flow parameters. This discrepancy is largely attributed to the pressure drop across the spacers. Use of best estimate flow parameters may significantly underestimate the resistance to laminar flow in the assembly, which leads to an overestimate of the cooling effects of naturally induced flows that develop in dry casks under normal storage conditions or wet pool cells during complete loss of coolant accidents.

Overestimating the cooling effects of naturally induced flows may lead to non-conservative analyses of dry cask performance and spent fuel pool accident consequences. Two geometric aspects unique to the BWR assembly somewhat mitigate this problem: 1) water rods in the center of the assembly carry a significant fraction of the total natural circulation flow and aid in cooling and 2) eight of the seventy-two rods in the 9×9 BWR assembly are partial length and end 1.32 m (52 in.) below the top of the assembly. The increased void space in this upper portion greatly reduces flow resistance in this region. These geometric aspects were not fully appreciated until close inspection of the prototypic

9×9 BWR components, whose specifications are concealed in proprietary vender drawings. This is one of the benefits obtained by the Sandia National Laboratories (SNL) spent fuel pool (SFP) experimental program's use of full-scale, prototypical vender hardware.

2 EXPERIMENTAL APPARATUS AND PROCEDURES

2.1 Fuel Assembly

The highly prototypic PWR fuel assembly was modeled after a commercial 17×17. Commercial components were purchased to create the assembly including the top and bottom nozzles, spacers, intermediate fluid mixers (IFM), 24 guide tubes, one central instrumentation tube, and all related assembly hardware. Many of these components are pictured in Fig. 1. The central instrumentation tube and guide tubes are permanently attached to the spacers to form the structural skeleton of the assembly. The top and bottom nozzles are removable. The 24 guide tubes are completely open through the top nozzle and completely blocked in the bottom nozzle. The outer diameter of the 24 guide tubes changes from 11.2 mm to 12.2 mm at an axial location 0.61 m from the bottom nozzle. Immediately above the guide tube diameter change are four 2.31 mm holes in the tube wall. The central instrumentation tube is the same diameter as the upper guide tubes and is the same diameter along the entire length. There are no holes in the instrumentation tube wall. The instrument tube is completely open through the bottom nozzle but is mostly blocked by the top nozzle with only a single 2.6 mm hole centered on the tube. If not blocked, the holes in the guide tube wall would allow some flow through the guide tubes. The majority of spent PWR have the guide tubes blocked by one of several special assemblies such as a thimble plug assembly, a control rod assembly or a burnable poison assembly. Unless noted otherwise, the data presented in this report are for blocked guide tubes.

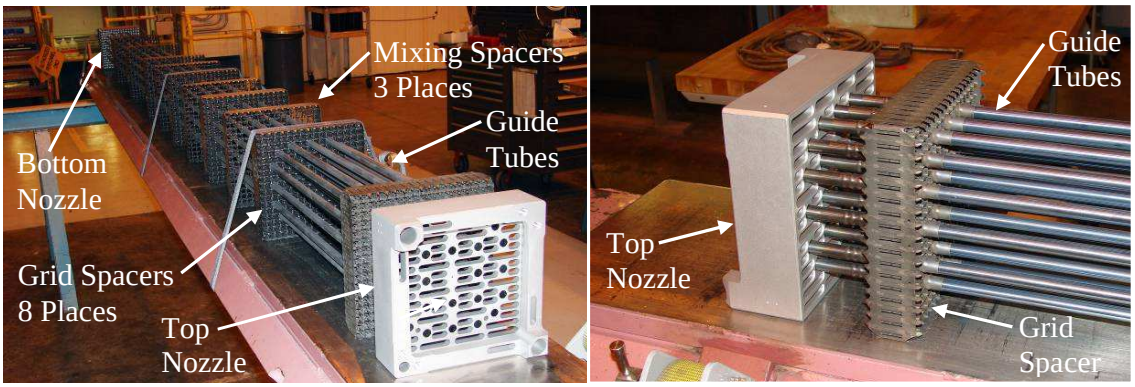

Fig. 1: Prototypic 17×17 PWR components.

Stainless steel tubing was substituted for the fuel rod pins for hydraulic testing. The diameter of the stainless steel rods was slightly larger than prototypic pins, 9.525 mm versus 9.500 mm. Prototypic fuel rod end plugs were press fit into the ends of the stainless tubing. The dimensions of the assembly components are listed in Table 1.

Fig. 2 shows the rod configuration of a typical 17×17 PWR assembly. Three different storage cells characterized by an inner dimension D_{cell} were studied. These cells are discussed next.

2.2 Storage Cells

A major difference between BWR and PWR assemblies is the absence of the channel box in the PWR. Without a channel box component, the pool or cask storage cell defines the flow boundaries for the PWR assembly (*i.e.*, similar to a BWR canister). The gap between the outer row of rods and the inside cell wall influences the nature of flow inside the bundle. In order to study this effect, three different sized storage cells were tested. The three sizes were chosen to represent two common commercial sizes and one small cell size that minimized the annular flow much like the BWR canister. Table 2 lists the dimensions of cells used in three Holtec dry casks and one pool rack. The

outer dimension of the 17×17 spacer is 214.0 mm (8.43 in.) and represents the smallest possible storage cell that would fit on the assembly. The internal dimensions of the commercial cells range considerably from a low of 222.2 mm (8.75 in.) to a high of 229.9 mm (9.05 in.).

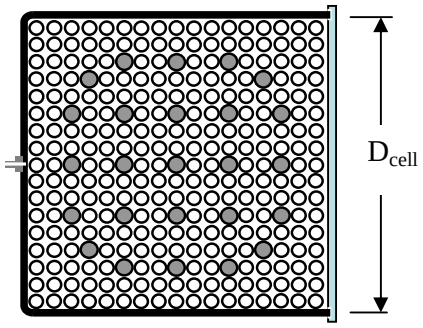

Fig. 2: Rod configuration of a typical 17×17 PWR assembly.

Table 1: Dimensions of assembly components in the commercial 17×17 PWR.

Description	Lower Section	Upper Section
Number of Pins	264	264
Pin Diameter (mm)	9.525	9.525
Pin Pitch (mm)	12.6	12.6
Pin Separation (mm)	3.025	3.025
Number of Instrument Tubes	1	1
Number of Guide Tubes (G/T)	24	24
G/T Diameter (mm)	11.2	12.2
Axial Length (m)	0.704	3.268

Since there is variation in the size of the cells used commercially, three different sized pool cells were tested as indicated in gray in Table 2 and depicted in Fig. 2 as dimension D_{cell}. The base case was the 217.5 (8.56 in.) cell with minimal annular flow area. Although this size is not found commercially, it is an important case for comparison purposes as it minimizes the complexity of the annular gap flow. The two other experimental storage cell sizes are 221.8 mm (8.73 in.) similar to that found in the Holtec MPC-24E/EF cask and 226.6 mm (8.92 in.) like that found in the Holtec MPC-24 cask. This span of sizes includes the size used in a typical Holtec spent fuel pool rack.

Table 2: Internal dimensions of commercial cask, pool cells and areas as-built experimental cell.

	Number in Cask	D_{cell} Length (mm)	Width (mm)	Experimental Storage Cell Dimension (mm)	Minimum Annular Gap (mm)
17×17 spacer	-	214.0	214.0	217.5	1.75
MPC-32	22	223.3	223.3		
	8	223.3	227.1		
	2	227.1	227.1		
MPC-24E/EF	20	222.2	222.2	221.8	3.9
	4	229.9	229.9		
MPC-24	24	226.6	226.6	226.6	6.3
Holtec pool	-	224.8	224.8		

2.3 Air Flow Control

Air was metered into the bottom of the assembly with eight mass flow controllers (MKS Instruments Inc. Model 1559A). The upper flow ranges of each controller are listed in the table inset in Fig. 3. Fig. 3 also shows a diagram of the flow metering and flow straightening components as well as photographs of the equipment used. The metered air was conditioned to produce a uniform velocity profile at the inlet of the assembly. Using best engineering practice, the flow from all the flow controllers was routed through a baffled manifold to mix the flows and equally distribute flow to the

bottom of a square flow straightener. The flow straightener consisted of a course screen, followed by a plastic honeycomb, followed by a fine screen. The selection of straightening components and their placement are based on the results of Farell and Youssef (1996). However, the resulting profile was not measured.

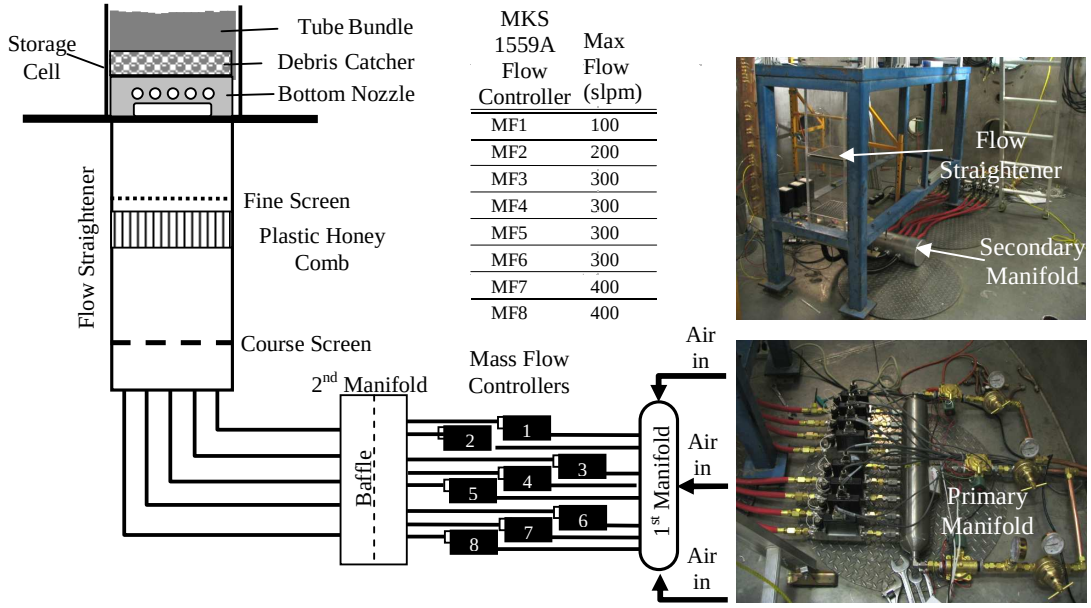

MKS 1559A Flow Controller	Max Flow (slpm)
MF1	100
MF2	200
MF3	300
MF4	300
MF5	300
MF6	300
MF7	400
MF8	400

Fig. 3: Diagram and photographs of the flow control and flow straightening systems.

2.4 Pressure Drop Measurements

Fig. 4 shows the layout of the PWR and BWR pressure drop experimental assemblies, including all available pressure port locations. Three Paroscientific Digiquartz differential pressure transducers (Model 1000-3D) were plumbed directly to the desired pressure ports. These pressure gauges use a highly sensitive quartz crystal to measure slight changes in differential pressure (resolution ~0.02 Pa). Unless noted otherwise, the measurements described hereafter were taken with the PWR guide tubes or BWR water rods blocked. These guide tubes were blocked at the top, which is open, by inserting tapered rubber plugs into each tube. Fig. 5 shows the lower section of the guide tube including the transition in the outer diameter and the location of the drain holes.

Measurements were recorded directly to the hard drive of a PC-based data acquisition system every 2 seconds using a LabView 8.2 interface. These measurements included the air flow rate through the assembly, ambient air temperature, ambient air pressure, and the assembly pressure drops. The LabView interface was used to automatically change the air flow rate according to a prescribed program which allowed a greater number of flow rates to be tested.

With each pressure transducer plumbed to two set port locations and with the air flow off, pressure drop measurements were recorded for a period of roughly 1 minute. These measurements were termed zero flow measurements and allowed for correction of any zero drift in the transducer. Next, the air flow was set to the desired rate with pressure drop readings subsequently acquired for 2 minutes. The air flow was then stopped, and zero flow measurements were again taken for 1 minute. This procedure was repeated for different air flow rates. The pressure spikes evident during the reestablishment of flow are discarded before averaging for the pressure drops. Also, the slight zero drift of the transducer was corrected by subtracting the average of the zero flow measurements taken prior to and after each respective flow test. The zero corrections of the pressure drops were less than 0.92 N/m^2, which occurred during an overall A–36 pressure drop measurement.

Additionally, the BWR characterized in a previous study was re-tested using the improved automated procedures described below (Lindgren and Durbin, 2007). The pressure port locations for the BWR assembly are also shown in Fig. 4.

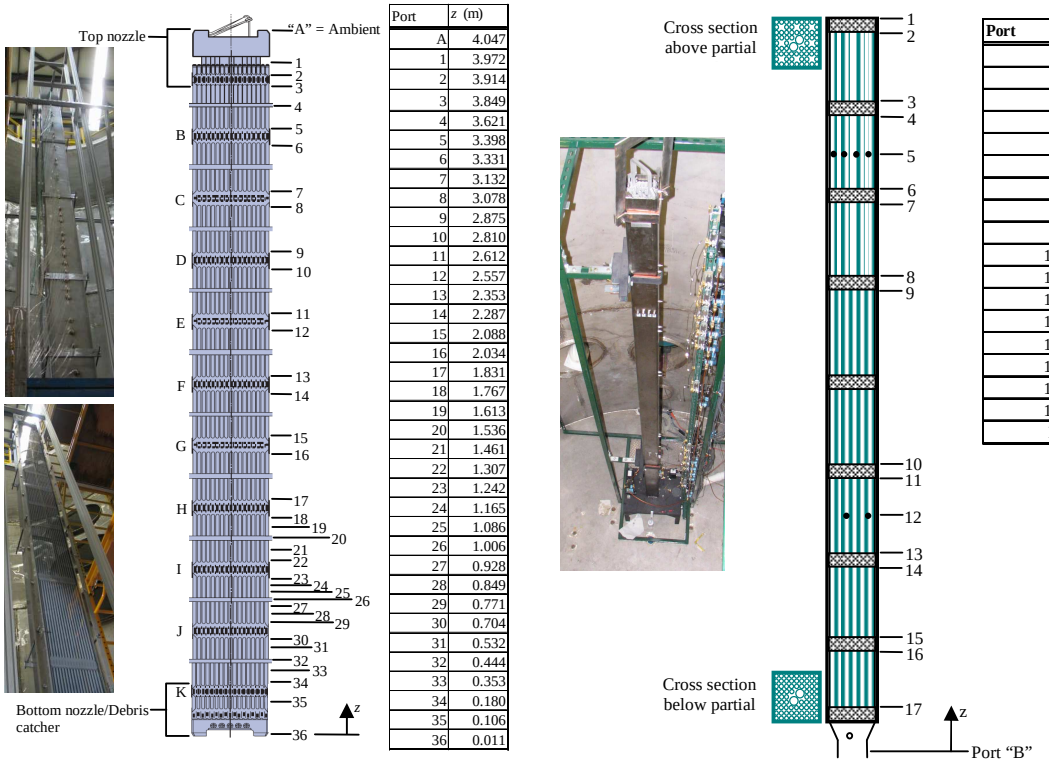

Port	z (m)
A	4.047
1	3.972
2	3.914
3	3.849
4	3.621
5	3.398
6	3.331
7	3.132
8	3.078
9	2.875
10	2.810
11	2.612
12	2.557
13	2.353
14	2.287
15	2.088
16	2.034
17	1.831
18	1.767
19	1.613
20	1.536
21	1.461
22	1.307
23	1.242
24	1.165
25	1.086
26	1.006
27	0.928
28	0.849
29	0.771
30	0.704
31	0.532
32	0.444
33	0.353
34	0.180
35	0.106
36	0.011

Port	z (m)
1	4.19
2	4.15
3	3.73
4	3.69
5	3.45
6	3.22
7	3.18
8	2.71
9	2.66
10	1.68
11	1.64
12	1.41
13	1.17
14	1.13
15	0.66
16	0.62
17	0.13
B	0.00

Fig. 4: Experimental PWR (left) and BWR (right) apparatuses showing as-built port locations.

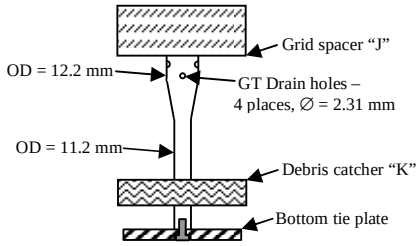

Fig. 5: Lower detail of the PWR guide tube.

3 DATA ANALYSIS

3.1 Overall Pressure Drop Dependence on Reynolds Number

Fig. 6 shows the overall assembly pressure drop as a function of Reynolds number in the bundle of the PWR (A–36) and BWR (1–B) assemblies. The BWR data is included for comparison and includes the new data collected in the present study along with the data collected in a previous study (Lindgren and Durbin, 2007). Data for the PWR assembly is shown for all three storage cells tested. The water rods in the BWR and the guide tubes in the PWR are plugged. For the smallest, 217.5 mm PWR storage cell that is sized to be analogous to the BWR canister, the pressure drop across the PWR is significantly larger than across the BWR assembly at all Reynolds numbers. For the 221.8 mm PWR storage cell, pressure drop across the PWR is similar to the pressure drop across the BWR assembly at all Reynolds numbers. The pressure drop across the BWR assembly is slightly lower than the pressure drop across the PWR assembly at low Reynolds numbers and nearly equal at higher Reynolds numbers. For the largest 226.6 mm PWR storage cell, the pressure drop across the PWR is significantly less than the pressure drop across the BWR assembly at all Reynolds numbers.

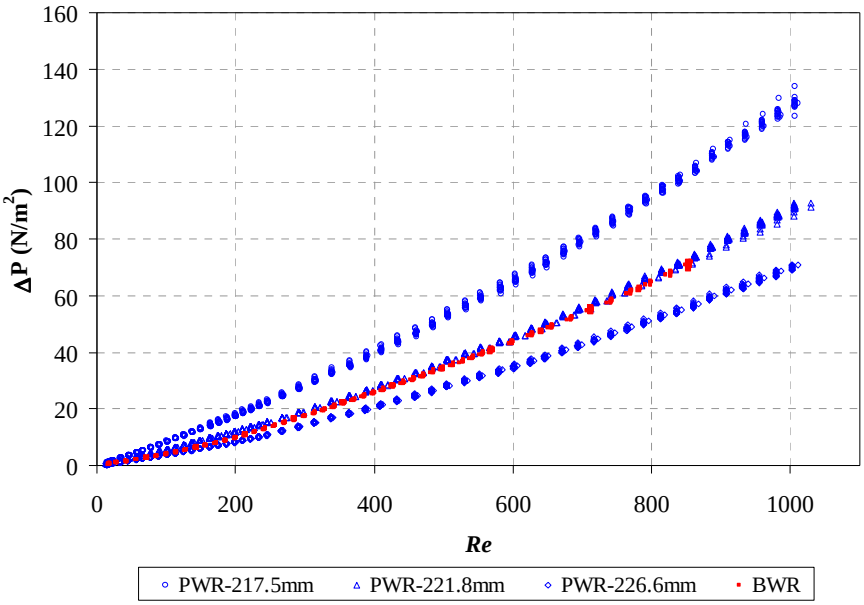

Fig. 6: Assembly pressure drop as a function of Reynolds numbers for analogous PWR and BWR fuel bundles.

3.2 Pressure Drop with Axial Position

Fig. 7 shows the axial pressure drop in a PWR assembly for three different flows when placed inside the smallest storage cell. The size of this storage cell is comparable to the canister on a BWR assembly. The pressure drop measured in the BWR assembly is shown for comparison. The pressure drop in the PWR is significantly higher than in the BWR assembly. The pressure drop along the PWR bundle and across the PWR spacers is slightly greater than the corresponding locations in the fully populated lower section of the BWR assembly and significantly greater than in the upper partially populated section of the BWR assembly.

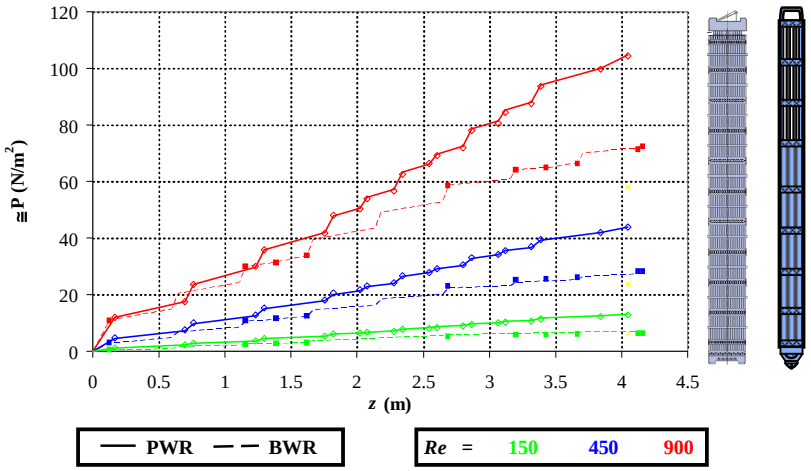

Fig. 7: Assembly pressure drop as a function of axial height for analogous PWR and BWR fuel bundles.

3.3 Hydraulic Loss Coefficient Analysis

The goal of this research was to determine the hydraulic coefficients for viscous or major loss, S_{LAM}, and form or minor loss, k, for use with thermal-hydraulic modeling. The cross-sectional areas and hydraulic diameters used in the hydraulic analyses to follow are presented in Table 3.

Table 3: Summary of the flow areas and hydraulic diameters of the hydraulic characterization experiments.

Description	Storage Cell Dimension (mm)	Flow Area (m^2)	D_H (m)
PWR Upper Bundle	217.5	0.0256	0.0105
PWR Lower Bundle	217.5	0.0260	0.0108
PWR Upper Bundle	221.8	0.0275	0.0113
PWR Lower Bundle	221.8	0.0279	0.0116
PWR Upper Bundle (Unblocked Guide Tubes)	221.8	0.0299	0.0113
PWR Lower Bundle (Unblocked Guide Tubes)	221.8	0.0279	0.0116
PWR Upper Bundle	226.6	0.0296	0.0121
PWR Lower Bundle	226.6	0.0301	0.0124
BWR Upper (Partially Populated)	132.6	0.0106	0.0141
BWR Lower (Fully Populated)	132.6	0.0098	0.0119

Curve fits to the pressure drop data were used to determine the S_{LAM} and k coefficients of the assembly. The technique used to determine these coefficients was successfully validated by investigation of flow in a simple annulus for which an analytic value of S_{LAM} is known. The determination of these coefficients is discussed next. The major, or viscous, pressure loss is expressed in Equation 1.

$$\Delta P_{major} = f\left(\frac{L}{D_H}\right)\left(\frac{\rho \cdot V_{Assembly}^2}{2}\right) \tag{1}$$

The friction factor for laminar flow is written explicitly as

$$f = \frac{S_{LAM}}{Re}, \text{ where } S_{LAM} = 64\,(\text{pipe flow}) \tag{2}$$

Substituting for the Reynolds number yields

$$\Delta P_{major} = S_{LAM}\left(\frac{L}{D_H^2}\right)\left(\frac{V_{Assembly} \cdot \mu}{2}\right) \tag{3}$$

The minor, or form, pressure drops across the assembly are given by

$$\Delta P_{minor} = \sum k\left(\frac{\rho \cdot V_{Assembly}^2}{2}\right) \tag{4}$$

Curve fits to pressure drop data are presented in the following format. In Equation 5, the quadratic term accounts for the minor losses and the linear term for the major losses.

$$\Delta P_{total} = a_2 \cdot V_{Assembly}^2 + a_1 \cdot V_{Assembly} \tag{5}$$

Because the total pressure drop is simply the sum of the major and minor pressure drops, the S_{LAM} and k coefficients may now be determined explicitly.

$$S_{LAM} = 2 \cdot a_1\left(\frac{D_H^2}{L \cdot \mu}\right)$$
$$\sum k = \frac{2 \cdot a_2}{\rho} \tag{6}$$

The analysis assumes air properties at local ambient conditions, typically ρ = 0.98 kg/m^3 and μ = 1.85×10^{-5} N·s/m^2. Changes in air temperature and pressure are taken into account for measurements collected during different experimental runs.

3.3.1 PWR Hydraulic Loss Coefficients

A summary of the S_{LAM} and k coefficients for all three PWR storage cells tested is shown in Table 4. These values were determined from the full experimental flow rate range of 30 to 2100 slpm, or Reynolds numbers of 10 to 1000, respectively. The hydraulic diameter and flow area of the upper section was used to calculate the S_{LAM} and k values. The S_{LAM} coefficient for the average bundle run and average spacer was calculated as the length weighted average. The k coeffiecient for the average bundle and spacer was calculated as the arithmetic average. Long and short bundle runs were averaged together as were regular and IFM spacers. Uncertainties in the S_{LAM} and k coefficients listed in Table 4 were determined to be ±5 and ±1.4, respectively.

Table 4: S_{LAM} and k coefficients for the PWR assembly in the three storage cells tested.

Cell size=> D_h => Segment	**Description**	**L (m)**	**217.5 mm 0.0105 m S_{LAM}**	**217.5 mm 0.015 m Σk**	**221.8 mm 0.0113 m S_{LAM}**	**221.8 mm 0.0113 m Σk**	**226.6 mm 0.0121 m S_{LAM}**	**226.6 mm 0.0121 m Σk**
A-3	Top Nozzle	0.2097	107.1	1.5	113.2	1.4	89.9	1.4
3-5	Long Bundle	0.4509	76.1	1.4	65.6	1.2	65.7	1.4
5-6	Spacer	0.0667	418.4	2	357.6	1.9	303.4	1.6
6-7	Short Bundle	0.199	82.4	1	57.7	0.9	52	0.7
7-8	IFM	0.0545	283.2	1.4	231.2	1.1	227.7	1
8-9	Short Bundle	0.2021	77	0.4	56	0.5	51.7	0.5
9-10	Spacer	0.0656	466.3	1.9	364.6	1.5	269.2	1.6
10-11	Short Bundle	0.1979	81.1	0.8	68.3	0.9	57.3	1.1
11-12*	IFM	0.0545	290.8	1.4	237.2	1.1	194.3	1
12-13*	Short Bundle	0.2043	77.2	0.7	50.7	0.5	53.3	0.6
13-14	Spacer	0.0661	432.1	2	394.9	1.9	302.1	1.8
14-15	Short Bundle	0.1995	72.1	0.8	57.4	0.7	53.9	0.8
15-16	IFM	0.0534	294.2	1.5	276.7	1.4	223.1	1.2
16-17	Short Bundle	0.2027	73.3	0.3	47.5	0.3	45.7	0.4
17-18	Spacer	0.0646	492.5	1.9	383.5	1.8	341.9	1.8
18-22	Long Bundle	0.4604	80.7	1	62.4	1.2	56	1.2
22-23	Spacer	0.0646	480	1.6	366.7	1.8	322.7	1.6
23-29	Long Bundle	0.471	77.2	1.5	65.4	1.5	60	1.7
29-30	Spacer	0.0667	424.3	2.2	314.5	1.3	296.7	1.6
30-34	Long Bundle	0.5244	77.4	0.5	73	1.6	68.1	1.5
34-36	Bottom Nozzle	0.1688	284.7	4.9	238.7	3.4	223.5	3.3
A-36	Overall (meas.)	4.0472	132.9	30.6	109.9	27.7	98.5	27.4
	Average Bundle		77.6	0.8	62.7	0.9	58.6	1.0
	Average Spacer		404.5	1.8	329.8	1.5	279.3	1.5

Due to a blockage in port 12, segments 11-12 and 12-13 values are averages of the remaining IFM spacers and short bundle segments, respectively.

For the smallest 217.5 mm storage cell the directly observed value of S_{LAM} for the overall pressure drop was 132.9. The directly measured value of Σk was 30.6. For the length weighted average bundle run and spacer the S_{LAM} was 77.6 and 404.5 respectively while Σk was 0.8 and 1.8 respectively.

For the 221.8 mm storage cell the directly observed value of S_{LAM} and Σk was 109.9 and 27.7 respectively. For the average bundle run and spacer the S_{LAM} was 62.7 and 329.8 respectively while Σk was 0.9 and 1.5 respectively.

For the 226.6 mm storage cell the directly observed value of S_{LAM} and Σk was 98.5 and 27.4 respectively. For the average bundle run and spacer the S_{LAM} was 58.6 and 279.3 respectively while Σk was 1.0 and 1.5 respectively.

3.3.2 BWR Hydraulic Loss Coefficients

A summary of the SLAM and k coefficients for the BWR assembly with blocked water rods is shown in Table 5. These measurements repeat those conducted in 2005 at SNL but include a more refined flow control capability. The hydraulic loss coefficients calculated in the present investigations are within the experimental error from those determined previously (2005 – SLAM = 106, k = 37) (Lindgren and Durbin, 2007). These values were determined from the full experimental flow rate range of 15 to 600 slpm, or Reynolds numbers of 20 to 850, respectively. The hydraulic diameter and flow area of the upper and lower sections of the BWR assembly are listed in Table 3. The hydraulic diameter and flow area of the lower fully populated bundle section was used to calculate the SLAM and k. The directly observed value of S_{LAM} for the overall pressure drop was 104.2. The directly measured value of Σk for the overall assembly pressure drop was 37.8. The length weighted average bundle run and individual spacer S_{LAM} was 75.1 and 722.2 respectively. The average k for the individual bundle run and spacer was 0.8 and 3.3 respectively.

Table 5: Full Flow Range S_{LAM} and k coefficients for the BWR assembly with blocked water rods.

D_h => Segment	**Description**	**L (m)**	**0.0119 m S_{LAM}**	**0.0119 m Σk**
1-2	Top Tie	0.04	44.4	0.4
2-3	Long Bundle	0.411	34.8	0.3
3-4	Spacer	0.044	313.3	2.6
4-6	Long Bundle	0.468	38.5	0.9
6-7	Spacer	0.042	298.6	2.6
7-8	Long Bundle	0.469	48	0.5
8-9	Spacer	0.044	733.6	3.4
9-10	2×Long Bundles + Spacer	0.98	105.4	5
10-11	Spacer	0.044	707.7	3.4
11-13	Long Bundle	0.467	77.2	0.9
13-14	Spacer	0.044	720.3	3.3
14-15	Long Bundle	0.468	75.1	0.8
15-16	Spacer	0.043	739.1	3.3
16-17	Long Bundle	0.47	73	0.7
17-B	Bottom Tie	0.127	124.5	10
Summation	Overall (equiv.)	4.19	--	38.1
1-B	Overall (meas.)	4.19	104.2	37.8
	Average Bundle		75.1	0.8
	Average Spacer		722.2	3.3

3.3.3 PWR Storage Cell Size Dependence

Three different sized PWR storage cells were tested to determine the effect of the storage cell size on the hydraulic viscous and form loss parameters. The smallest storage cell tested was 217.5 mm and is constrained by the size of the spacer, which is 214 mm. The other two storage cells tested were 221.8 mm and 226.6 mm, which span the sizes of the most common storage cells. The largest storage cell found in the three dry casks considered is 230 mm.

The geometry of the annular flow path is different in each of the storage cells. The hydraulic diameter of the storage cell increases as the flow area of the annular region increases. This change in annular flow areas between different storage cells affects the distribution of flow between the bundle and annular regions. The hydraulic loss parameters are also affected. Fig. 8 shows the dependence of the overall S_{LAM} and Σk on the storage cell hydraulic diameter based on data from the full range of laminar flows (*Re* = 10 to 1000) for the overall assembly length.

The full-flow-range S_{LAM} drops from 134.0 at D_H = 0.0105 m (217.5 mm cell) to 110.7 at D_H = 0.0113 m (221.8 mm cell) to 98.6 at D_H = 0.0121 m (226.6 mm cell). An empirical power law correlation was developed to aid in assigning hydraulic parameters to storage cell sizes not tested. The validity of this correlation is limited to 17×17 PWR fuel. In the limit as the cells size increases, the S_{LAM} should asymptotically approach the value of 57 for a square duct [Kays and Crawford, 1980, Fig 6-4, p. 63]. A power law correlation was chosen because it could be forced to approach this limiting value.

The full-flow-range form loss coefficient, Σk, shows less dependence on cell size. For D_H = 0.0105 m (217.5 mm cell), k is 30.9 and drops to 28.0 at D_H = 0.0113 m (221.8 mm cell) and 27.8 at D_H = 0.0121 m (226.6 mm cell). A power law correlation was also used to fit the form loss data.

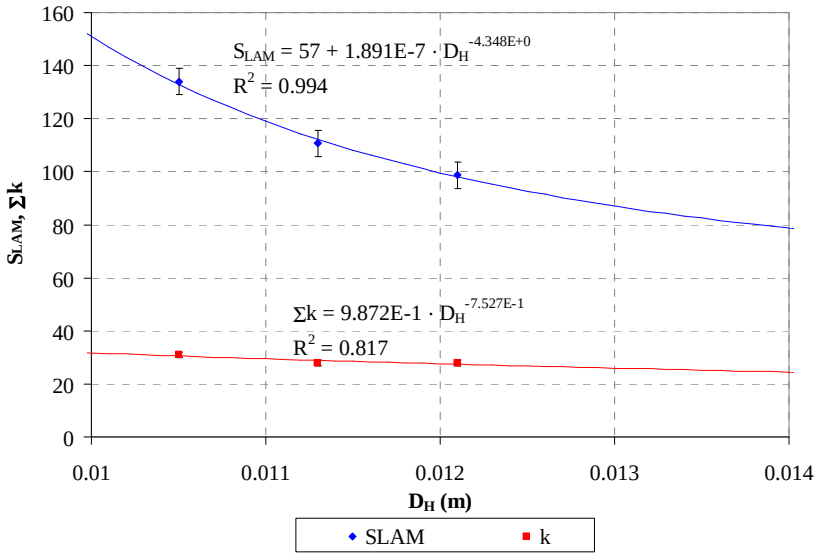

Fig. 8: Dependence of S_{LAM} and Σk on the hydraulic diameter for full flow range (*Re* = 10 to 1000) and overall assembly length. The validity of this correlation is limited to 17×17 PWR fuel.

Fig. 9 shows the dependence of the S_{LAM} (left) and k (right) on the storage cell hydraulic diameter for average individual bundle runs and spacers. The S_{LAM} for an individual spacer is much larger and more dependent on the hydraulic diameter than the S_{LAM} for an individual bundle run. For the individual spacer, the S_{LAM} drops from 405 with the smallest storage cell, to 315 in the mid-sized cell to 297 with the largest cell. The respective drop in S_{LAM} for and individual bundle run is from 78 to 63 to 59. Most of the hydraulic diameter dependence for the S_{LAM} for the overall assembly shown in Fig. 8 is evidently due to the spacers. As with the overall assembly, a power law correlation forced to approach 57 was developed to describe the dependence on hydraulic diameter.

The form loss coefficient k shows weak dependence on hydraulic diameter or cell size. For an individual spacer, k decreases slightly with D_H. For a bundle run, k increases slightly with D_H. The sum of an individual spacer and bundle run results in a D_H dependence very similar to that exhibited by the overall assembly as shown in Fig. 8.

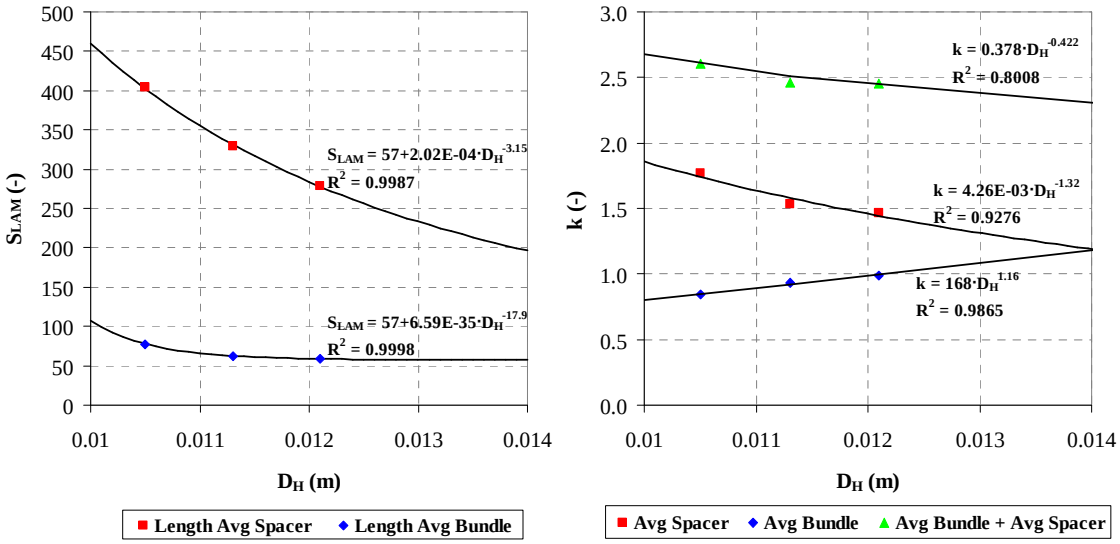

Fig. 9: Hydraulic diameter dependence of S_{LAM} (left) and k (right) for individual bundle runs and spacers for full flow range (*Re* = 10 to 1000). The validity of this correlation is limited to 17×17 PWR fuel assemblies.

4 SUMMARY

These studies represent the first hydraulic characterizations of a full length, highly prototypic PWR fuel assembly in low Reynolds number flows. A commercial 17×17 PWR fuel assembly was hydraulically characterized by measuring both pressure drops and velocities inside three different storage cells in the laminar regime. Two of the storage cell sizes (226.6 mm and 221.8 mm) were chosen to span the cell size commonly used in dry storage casks and the third size (217.5 mm) was chosen as a practical minimum that forced most the air flow through the tube bundle. These tests spanned Reynolds numbers from 10 to 1000 based on the hydraulic diameter and average assembly velocity. The pressure drop results were used to calculate viscous and form loss coefficients, namely S_{LAM} and Σk, respectively.

Pressure drop measurements were collected at 52 different flow rates between 25 and 2100 slpm. Three high precision quartz crystal differential pressure gauges collected data from 36 pressure ports. The pressure ports were positioned to allow characterization of all individual spacers and bundle runs along the axis of the assembly. Overall pressure drop data was used to calculate S_{LAM} and Σk hydraulic loss coefficients. The technique used to determine these coefficients was successfully validated by investigation of flow in a simple annulus for which an analytic value for S_{LAM} is known.

For reference, comparison was made with the BWR assembly characterized in a previous study. The BWR assembly was also re-tested, and the new pressure drop data is in excellent agreement with the previous study.

The smallest PWR storage cell tested (217.5 mm) is analogous to a BWR canister. The overall pressure drop across the PWR assembly in this storage cell was significantly greater than the overall pressure drop across the BWR assembly. The BWR pressure drop is lower because the assembly has fewer grid spacers, and partial length rods result in a significant increase in flow area in the upper third of the assembly. The overall S_{LAM} and Σk hydraulic parameters for the PWR assembly in the 217.5 mm storage cell were determined to be 133 and 30.6 respectively.

The middle sized PWR storage cell (221.8 mm) tested represents the smallest cell typically used in commercial dry casks. The overall pressure drop across the PWR assembly in the 221.8 mm cell was found to be essentially the same as the overall pressure drop across the BWR assembly. The overall

S_{LAM} and Σk hydraulic parameters for the PWR assembly in the 221.8 mm storage cell were determined to be 109.9 and 27.7 respectively.

The largest PWR storage cell tested (226.6 mm) represents the largest cell typically used in commercial dry casks. The overall pressure drop across the PWR assembly in the 226.6 mm cell was significantly lower than the overall pressure drop across the BWR assembly. The overall S_{LAM} and Σk hydraulic parameters for the PWR assembly in the 226.6 mm storage cell were determined to be 98.5 and 27.4 respectively.

The viscous loss coefficient, S_{LAM}, exhibits a larger dependence on storage cell hydraulic diameter than the form loss coefficient, Σk. To aid in determining the appropriate coefficients to use with storage cell sizes not tested, empirical power law correlations were determined for S_{LAM} and Σk as a function of storage cell hydraulic diameter. The resulting correlations based on the full range of flow rates tested (*Re* = 10 to 1000) are:

$$S_{LAM} = 57 + 1.891E\text{-}7 \cdot D_H^{-4.348} \quad (7)$$

$$\Sigma k = 9.872E\text{-}1 \cdot D_H^{-7.527} \quad (8)$$

where D_H is the storage cell hydraulic diameter in meters. The correlations should only be used for 17×17 PWR fuel assemblies with storage cells smaller than 226.6 mm.

5 REFERENCES

S. Cheng and N.E. Todreas, "Hydrodynamic Models and Correlations for Bare and Wire-Wrapped Hexagonal Rod Bundles—Bundle Friction Factors, Subchannel Friction Factors and Mixing Parameters," *Nucl. Eng. Des.*, **92**, 227-251 (1986).

A.M. DeStordeur, "Drag Coefficients for Fuel Elements Spacers," *Nucleonics*, **19**, 74 (1961).

C. Farell, and S. Youssef, 1996, "Experiments on Turbulence Management Using Screens and Honeycombs," *J. Fluids Eng.*, **118**, 26-32.

W.M. Kays, and M.E. Crawford, 1980, Convective Heat and Mass Transfer, Second Edition, New York, NY: McGraw- Hill.

E.R. Lindgren, and S.G Durbin, 2007, "Characterization of Thermal-Hydraulic and Ignition Phenomena in Prototypic, Full-Length Boiling Water Reactor Spent Fuel Pool Assemblies after a Complete Loss-of-Coolant Accident," SAND2007-2270.

K. Rehme, "Pressure Drop Correlations for Fuel Elements Spacers," *Nucl. Technol.*, **17**, 15-23 (1973).

N.E. Todreas and M.S. Kazimi, Nuclear Systems I, 382-386, (1990).